A Survey of Human Body Communication Transceivers: Design Challenges and Key Strategies

Qi Huang[1], Abdelhay Ali[2], Abdulkadir Celik[2], Gianluca Setti[2], Jaafar Elmirghani[3], Noha Al-Harthi[3], Khaled N. Salama[2], Shreyas Sen[1], Mohammed E. Fouda[4], and Ahmed M. Eltawil[2]

[1]Department of Electrical and Computer Engineering, Purdue University, West Lafayette, IN, USA.
[2]Electrical and Computer Engineering at King Abdullah University of Science and Technology, Saudia Arabia
[3]Neom, Saudi Arabia
[4]Compumacy for Artificial Intelligence Solutions, Cairo, Egypt.
[*]e-mail: ahmed.eltawil@kaust.edu.sa

ABSTRACT

While advances in medicine have facilitated access to treatments and preventative protocols, providing holistic care continues to require multiple doctor visits, disrupting daily routines and burdening medical infrastructure. The Internet of Bodies (IoB), which integrates wearable, implantable, ingestible, and injectable devices in, on, and around the body, offers a promising solution by enabling real-time monitoring of health conditions and disease progression and enhancing early intervention opportunities. IoB has progressed significantly due to advances in miniaturized electronics, flexible substrates, and low-power design. A key area of interest is human body communication (HBC), where the human body serves as the communication medium. By replacing the radio front-end with simple direct skin interfaces, sensing and communication modules become smaller, lighter, more energy-efficient, and accessible. This review presents an in-depth overview of the challenges, strategies, and future directions in HBC transceiver design, covering the fundamental principles of electrical field HBC. Design challenges such as dynamic channel variations, skin-electrode interfaces, operational frequency, interference, safety, and reliability are discussed. Additionally, the review explores circuit design techniques and the potential of artificial intelligence to enhance HBC system efficiency. It concludes with insights outlining potential avenues for future research in the field of HBC.

1 Introduction

Taking a cue from the Internet of Things (IoT), the Internet of Bodies (IoB) is defined as a network of smart objects distributed in, on, and around the human body[1]. Having its roots in Wireless Body Area Networks (WBANs), the IoB is a network of wearable, implantable, ingestible, and injectable devices that have become possible due to simultaneous advancements in microelectronics, signal processing, and wireless communications. Various applications of IoB exist, as shown in Fig. 1, including wearable devices such as smartwatches, diabetes management systems, and motion detectors[2–4], where devices can measure vital signs such as heart rate, blood pressure, and sweat pH[5,6]. Ingestible devices, such as wireless capsule endoscopes, can be used for gastrointestinal examinations[7], while implantable devices such as pacemakers and brain-machine interfaces can provide medical interventions[8,9]. Subdermal devices offer heart activity monitoring and identity recognition capabilities[10]. By providing continuous access to such information, IoB has the potential to revolutionize numerous sectors, including healthcare, personalized medicine, public safety, smart-home-assisted independent living, occupational health and safety, wellness, fitness, sports, and entertainment.

Meeting the diverse demands of IoB applications requires addressing different design objectives, including compact size, affordability, extremely low power consumption, high reliability, minimal delay, security, and convenience. This translates into Size, Weight, and Power-Cost (SWaP-C) constraints, primarily influenced by battery size and circuit area. Maximizing IoB node lifetime relies on low-power transceiver architecture with simplified hardware design. Balancing low power and low complexity impacts the device size, crucial for comfortable integration on or inside the body, while meeting Quality of Service (QoS) and Quality of Experience (QoE) requirements. For example, a wireless capsule endoscope requires over eight hours of operation for a complete intestinal examination[11], while implanted devices must exhibit reliable performance over many years. Strategies such as current reusing, replacing power-hungry elements, duty-cycling, and power-efficient architectures help achieve low power. However, these strategies might conflict with the ultra-reliable and low-latency communication requirements of time-sensitive IoB applications.

Safety and security requirements pose additional challenges to SWaP-C constraints. For example, IoB devices have to limit

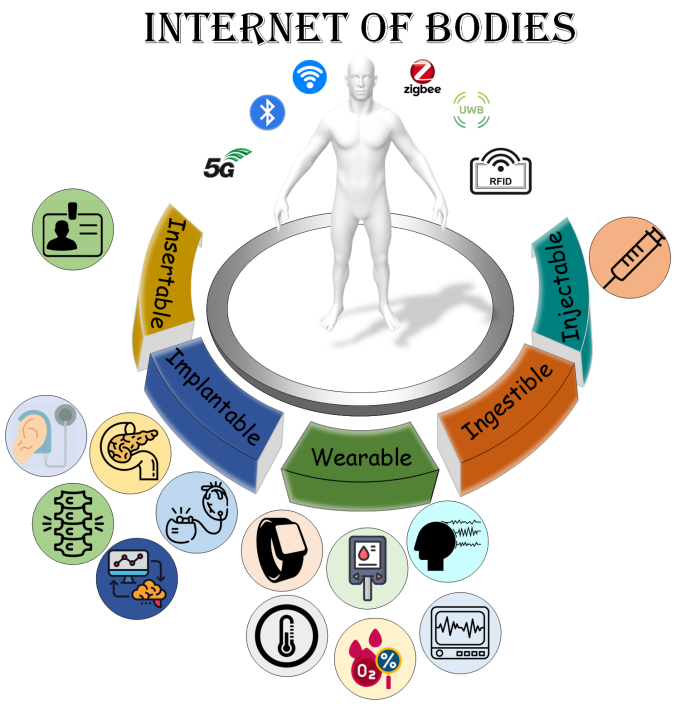

Figure 1. Illustration of insertable wearable, implantable, ingestible, and injectible IoB devices

time-varying electromagnetic field exposure of the human body under a Specific Absorption Rate (SAR) expressed in units of watts per kilogram. In addition, the electric current applied to the human body must be below the safety exposure reference levels specified in health regulation standards[12,13]. In particular, invasive IoB devices must also comply with the safety, efficacy, and security requirements set by public health and safety regulators such as the Food and Drug Administration (FDA). Finally, hardware and packaging design should be reliable, durable, and bio-compatible for in-body IoB devices. On the other hand, wearable IoB devices should be designed for comfort and safety, leveraging emerging technologies such as stretchable, textile, and inkjet-printable electronics, etc.

The emerging field of human body communication (HBC) is challenging the dominance of RF-based health wearables for numerous reasons including[1]: 1) RF signals are highly radiative and omnidirectional, resulting in energy loss and vulnerability to eavesdropping and malicious attacks, 2) RF-based IoB devices require substantial circuit area and battery capacity for radio front-ends, imposing strict SWaP-C design constraints, and 3) RF devices operating in license-free ISM bands can cause interference to IoB devices, especially with the increasing number of IoT devices. In contrast, HBC utilizes the body as a transmission medium (in-lieu of RF), ensuring physically secure connections with low signal leakage compared to RF bands[14]. HBC benefits from the body's conductivity, resulting in lower path loss and reduced transmission power requirements[15]. HBC also exhibits higher reliability than RF-based channels due to minimized RF shadow fading effects caused by body postures[1,16]. These features make HBC suitable for achieving ultra-low-power, low-cost, and low-complexity transceiver designs that meet the throughput and energy efficiency needs of IoB applications while adhering to SWaP-C constraints. State-of-the-art HBC transceivers demonstrate impressive energy efficiency levels as low as 2.24 pJ/bit[17], a significant improvement over commonly used RF-based devices.

Table 1. RF Communication Techniques

Communication	Bluetooth	BLE	Zigbee	Z-wave	ANT	NFC	RFID
Standardization	IEEE 802.15.1, now by Special Interest Group (SIG)	IEEE 802.15.1	IEEE 802.15.4	Proprietary	Proprietary	ISO/IEC 14443 etc.	ISO 18000 etc.
Topology	Mesh	Point-to-point, star, mesh	Mesh	Mesh	Point-to-point, star, tree, mesh	Point-to-point	Peer to peer
Band	2.4 GHz	2.4 GHz	Mainly 2.4 GHz	2.4 GHz and 900 MHz	2.4 GHz	13.56 MHz	125∼134 kHz 13.56 MHz 433 MHz, 860∼960 MHz, 2.45 GHz, 5.8 GHz
Range	1∼100 m	10∼600 m	10∼100 m	10∼100 m	Within 100 m	Within 20 cm	Within 100 m
Maximum data rate	3 Mbps	2 Mbps	250 kbps	100 kbps	60 kbps	0.848 Mbps	100 kbps

Numerous surveys have examined various aspects of IoB/WBAN and HBC, including potential applications, propagation characterization, channel modeling, antenna design, body coupling mechanisms, development trends, challenges, electrode modeling, and impedance modeling[1,16,18–31]. However, there is a notable gap in the literature when it comes to a comprehensive review that focuses specifically on design approaches and insights unique to HBC transceiver architectures. This review aims to fill this gap by providing a systematic and comprehensive survey of HBC design requirements and challenges, state-of-the-art HBC transceiver architectures, and key strategies, while also offering valuable insights into future research directions. To the best of the authors' knowledge, this work represents the first of its kind in this specific area, contributing significantly to the advancement and understanding of HBC technology. Specifically, this review addresses the following topics:

- Provides a comprehensive summary of popular intra-body communication techniques utilized in WBANs,
- Conducts a thorough survey of the design considerations for reliable and efficient HBC transceivers,
- Presents a comprehensive survey of key design strategies and techniques derived from the literature for Capacitive Coupling HBC (CC-HBC), and
- Identifies challenges and unresolved issues in the field of HBC and offers valuable insights outlining the potential avenues for future research.

2 Intra-Body Communication Techniques

This section delves into various intra-body communication strategies designed to navigate the broad IoB design space. Initially, we review the RF physical (PHY) layer of the IEEE 802.15.6 standard, encompassing both the NB PHY layer and UWB PHY layer. Following, we provide a summary of other prevalent RF communication methods such as Bluetooth, Zigbee, Z-wave, ANT, NFC, and RFID. A comparative study is performed on intra-body communication methods that employ HBC variations. This review aims to explore the practical aspects and features of these methods.

2.1 IEEE 802.15.6 Standard

The IEEE 802.15.6 standard is an international standard for WBANs, emphasizing low-power, short-range, and reliable wireless communications near the human body[32]. It encompasses multiple frequency bands, including Narrowband (NB), Ultra-Wideband (UWB), and HBC. NB operates in licensed and unlicensed bands such as 402-405 MHz, 420-450 MHz, among others. UWB supports a default and high QoS mode, with frequencies spanning from 3494.4 MHz to 9984.0 MHz, facilitating high data rate transmissions and precise location tracking[33]. HBC utilizes frequencies below 100 MHz for transmissions directly through the human body, ideal for devices in contact with the skin.

The standard also covers frequencies for specific services, such as the Medical Implant Communication Service (MICS), Wireless Medical Telemetry Service (WMTS), and Industrial, Scientific, and Medical (ISM) bands. Notably, these services are not part of IEEE 802.15.6 but were developed by the medical community, regulated in the U.S. by the Federal Communication Commission (FCC) to minimize interference risks. MICS is allocated the 402-405 MHz band for communication between medical implants and external devices, while WMTS uses designated bands (608-614 MHz, 1395-1400 MHz, 1427-1432 MHz) for transmitting medical telemetry data in a controlled environment[34]. The ISM band, crowded with IoT devices, benefits from UWB's high data rate capabilities and power efficiency, enhancing the longevity of IoB devices[35].

2.2 Other RF Communication Techniques

The IEEE 802.15.6 targets high reliability and robustness in challenging environments, such as those involving body movement and various obstructions typical in medical settings. However, for short-range device-to-device communication, numerous other RF standards have found wide-range acceptance. Table 1 provides a summary of the main features of these communication techniques, including their standardization status, topology, frequency band, range, and maximum data rate. In the following, we provide a brief overview of common RF standards used in IoB context.

- Bluetooth, introduced in 1998 and operating between 2.40 GHz to 2.48 GHz in the ISM band, supports enhanced connectivity with advancements such as Bluetooth v6.x, achieving up to 240 meters range and 100 Mbps data rates[36]. Introduced in Bluetooth 4.0, Bluetooth Low Energy (BLE) significantly improves energy efficiency through techniques like duty cycling, making it vital for wearable health devices and real-time patient monitoring[37,38].
- Zigbee operates over 10m-100m range and excels in low-rate data communication. It is more energy-efficient and has quicker mode-switch latency than classic Bluetooth, though BLE surpasses it in power efficiency[39,40]. Secure through access control list (ACL) and Advanced encryption standard (AES), Zigbee is mainly found in network-rich environments like hospitals due to its mesh networking capabilities, rather than in consumer wearables.

- Z-Wave operates at up to 100m range with typical data rates of 100 kbps. It supports robust mesh networking ideal for home automation applications like lighting and security. Known for its low power use and cost-effectiveness, Z-Wave thrives in larger network installations for health and wellness[41].
- ANT, an ultra-low-power multicast technology in the 2.40 GHz ISM band, supports various network topologies and adapts to many applications with its efficient power use and flexible network configuration. While less common in consumer health tech than BLE, ANT's connectivity and energy efficiency are favored for long-term monitoring devices[42].
- NFC operates at distances up to 10 cm, supporting data rates up to 848 Kbps. Widely used in payment and data sharing, NFC's role in health tech is growing, particularly in patient ID and device management via secure, easy communication[43].
- RFID technology spans several frequencies and is pivotal in healthcare for patient tracking and equipment management. RFID tags, ranging from passive to active, facilitate non-contact data transfer, improving patient care efficiency and enabling remote device monitoring[43,44].

While specific implementations may vary, Bluetooth generally demonstrates a good combination of higher data rates with lower power consumption, with efficiency in the 10 nJ/b[45]. NFC and ANT are typically around the 100 nJ/b[46], while Z-Wave and Zigbee are close to the 1 μJ/b[47]. Bluetooth, BLE, and UWB are particularly well-suited for scenarios requiring high data rates, such as medical images or audio transmissions. On the other hand, NFC, ANT, Zigbee, and Z-Wave are more suitable for applications with lower bit rates, such as vital sign monitoring, among others.

2.3 Human Body Communications

HBC provides an alternative to RF-based systems and offers several advantages over them. These advantages include reduced power consumption and a smaller area footprint, enhanced security, and the ability to overcome body shadowing effects that are commonly encountered by RF transceivers. To ensure standardized implementation, the IEEE 802.15.6 standard defines the HBC PHY layer requirements, which operates on a 5 MHz band centered at 21 MHz and supports a data rate of up to 1.3125 Mbps[48]. HBC can be broadly categorized into two types: *magnetic (mHBC) vs electrical (eHBC)*. Furthermore, eHBC can be further classified into two subcategories: Galvanic-Coupling HBC (GC-HBC) and Capacitive-Coupling HBC (CC-HBC), as illustrated in Fig. 2. Next, we discuss these communication techniques in more detail.

GC-HBC The GC-HBC system employs a pair of electrodes, namely the ground electrode and signal electrode, to transmit signals through the human body using the electric field. Both the signal and ground electrodes make contact with the human skin. GC-HBC is less affected by environmental factors and human postures, offering a stable signal path and channel conditions as both the forward and backward paths traverse the human body. This stability makes GC-HBC suitable for transmitting vital or physiological data in both in-body and on-body. However, it is important to note that galvanic coupling operates best in low-frequency bands due to the relatively low conductivity of tissues in the human body[49]. This limitation results in a restricted bandwidth, lower data rates (<1 Mbps), and a shorter communication range. Furthermore, in galvanic coupling, ionization may occur on the human skin, which can raise safety concerns when the system is in operation.

CC-HBC Unlike GC-HBC, CC-HBC deploys the signal electrode in contact with the human skin while the ground electrode remains floating in the air, forming a coupling pathway between the electrodes through the environment and the human body. However, it is important to note that CC-HBC is more susceptible to external interference, including human postures and environmental conditions, compared to GC-HBC[15]. On the other hand, CC-HBC has the advantage of operating in higher-frequency bands, allowing it to support high data rates. It also enables communication over longer distances with lower path loss compared to GC-HBC. Particularly, CC-HBC exhibits superior performance compared to GC-HBC[22] at frequencies above 60 kHz. Furthermore, recent studies have also conducted preliminary investigations into the potential of implanted CC-HBC, utilizing an isolated ground electrode[50]. Therefore, CC-HBC has received more attention and is currently being extensively investigated in the literature. Consequently, subsequent sections of this survey will focus on CC-HBC, providing a deeper exploration of its characteristics and the latest advances in research.

mHBC The concept of mHBC was initially proposed by Ogasawara et al. in 2015[51], followed by the introduction of an mHBC transceiver design proposed in[52]. As depicted in Fig. 2(c), mHBC utilizes TX and RX coils to generate and receive magnetic energy for data transmission. An effective loop is formed through the body when the feet are connected to the ground electrode and the hands touch the signal electrode, without which the loop remains open[52]. Compared to eHBC, mHBC takes advantage of the fact that the human body exhibits better permeability than conductivity at MHz frequencies. This allows the magnetic field to propagate freely within the body, yielding a lower path loss than eHBC. Additionally, the magnetic field can be sensed in a single-ended manner, leading to reduced hardware complexity. Moreover, the inherent filtering characteristics of the human body and inductive coil help reduce external interference from human postures and environmental variations[49].

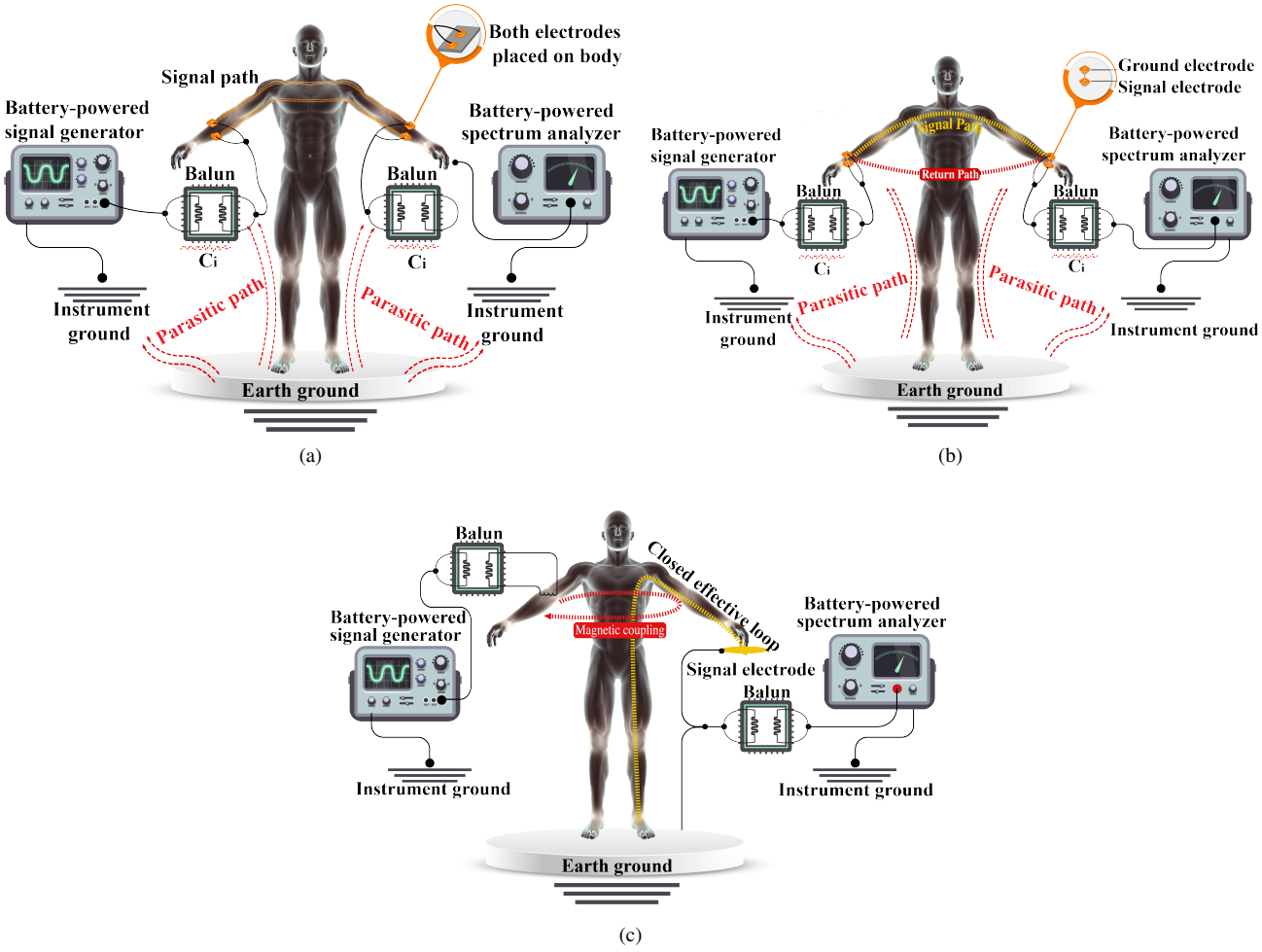

Figure 2. HBC coupling methods: a) galvanic coupling, b) capacitive coupling, and c) magnetic coupling.

Discussion In summary, each communication technique has a unique profile for channel loss and usage. eHBC provides the best combination of efficient hardware and reasonable channel loss, which is why eHBC is the most commonly used mode, particularly in health monitoring and fitness tracking applications. In contrast, mHBC generally incurs a more complicated hardware profile, resulting in lower adoption. RF communication, while versatile and capable of longer range, faces variable channel losses heavily influenced by frequency and environmental factors and subject to physical layer security vulnerabilities.

3 Design Considerations for HBC Transceivers

This section aims to provide a deeper exploration of CC-HBC's characteristics, challenges, and design considerations focusing on five essential topics in CC-HBC. First, we delve into the CC-HBC channel models and the safety standards to ensure the well-being of individuals exposed to electromagnetic fields.

3.1 HBC Channel

One crucial factor in the design of any communication system is the channel model. Specifically, we explore the significance of the body impedance, return path, and operating frequency in shaping the characteristics of the channel model.

CC-HBC Channel Model Modeling of CC-HBC channel can be approached through various methods, including analytical, numerical, and circuit models[1]. Among these approaches, circuit models offer an effective means of representing CC-HBC by utilizing equivalent RC components, resulting in simple transfer functions that mathematically describe the signal propagation along the transmission path within or on the human body. Circuit models provide several advantages in terms of computational efficiency and accuracy for a wide range of frequencies of interest; however, as the frequency reaches up to 100 MHz, radiative effects reduce the accuracy and alternative means such as full EM wave simulations may be needed.[1].

The CC-HBC channel can be divided into the forward and return paths, which are essential components determining the overall channel quality. The forward path consists of signal electrodes in contact with the skin, while the return path is formed by the coupling between the ground electrodes through the air and the body. The distance between the ground electrodes affects the capacitance, impedance, and channel quality. As the distance between the ground electrodes increases or decreases due to movements, the capacitance changes, consequently impacting the return path impedance and overall channel quality. Environmental factors, such as nearby metallic objects, temperature, humidity, pressure, and noise, can also influence the characteristics of the return path. Therefore, depending on the operation frequency, continuous monitoring and compensation of variable losses are crucial for optimizing and stabilizing the channel characteristics.

Circuit Model The equivalent circuit model of the CC-HBC channel, as presented in[53], is illustrated in Fig. 3(a). The CC-HBC channel model incorporates various capacitive and resistive components, each serving a specific role in the channel. The black line indicates the forward path for signal transmission through the human body, the red line is the backward path for ground coupling through the air, while the cyan line indicates cross-coupling paths between electrodes. The solid lines indicate the coupling through the human body, while the dashed lines indicate the coupling through air.

Effect of Impedances: Impedance components play a critical role in characterizing the CC-HBC channel. At frequencies lower than a few MHz in the Electro quasi-static (EQS) band, lumped circuit models can be used to describe the channel, where path loss is measured by the ratio of the received voltage to the transmitted voltage. It is desirable to minimize source impedance and maximize the load impedance to reduce voltage loss. As shown in Fig. 3(b), the forward path of the HBC channel can be represented by an internal resistance of the voltage source R_{Tx}, the body channel impedance Z_{body}, and the receiver termination impedance Z_{Rx}. The return path can be modeled with the return path capacitance C_{ret}. A simplified relationship between the output voltage V_{out} and the input voltage V_{in} can be expressed as[53]:

$$\frac{V_{out}}{V_{in}} = \frac{Z_{Rx}}{R_{Tx} + Z_{body} + Z_{Rx} + \frac{1}{sC_{ret}}} \tag{1}$$

A higher receiver impedance is preferred as it results in more voltage applied at the receiver end. The received voltage V_{out} increases with higher receiver input impedance (Z_{Rx}), leading to a smaller path loss. Therefore, avoiding a 50 Ω device impedance at the receiver end is preferable, as it may result in higher voltage loss through the body channel[53]. Conversely, a lower transmitter internal impedance should be used to reduce path loss.

Compared to resistive termination, capacitive termination offers several advantages, including lower path loss, wide bandwidth and flat path loss pattern. The channel loss of capacitive termination can be expressed by $\frac{C_{ret}}{C_{ret}+C_{load}}$[55]. As shown in Fig. 3(b), as the transfer function remains constant, the path loss remains flat across the frequency band of interest. Therefore, the channel loss is primarily determined by the ratio of the load capacitance to the return path capacitance[53]. A larger value of

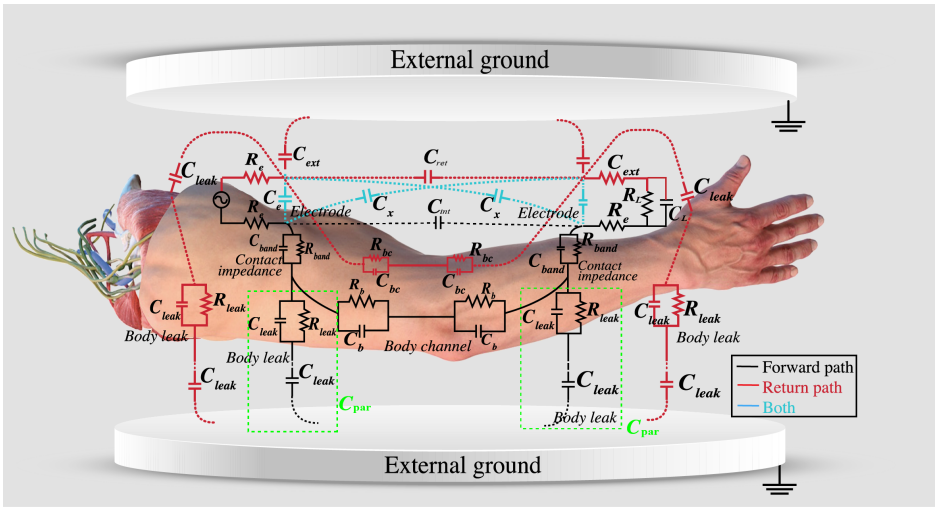

(a)

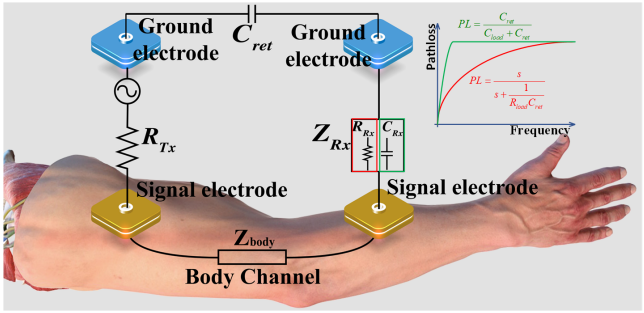

(b)

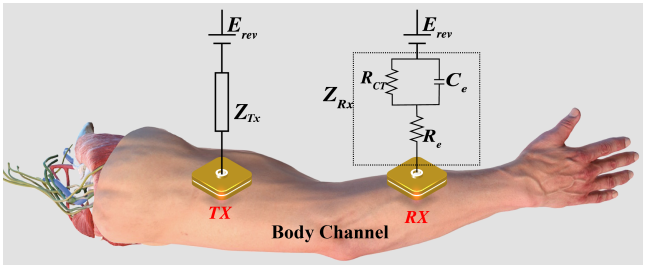

(c)

Figure 3. (a) Circuit model diagram for CC-HBC[54]. the definitions of the circuit model parameters are presented in the supplementary materials Table. 1. (b) Simplified CC-HBC channel circuit models[55,56], and (c) Electrode-Skin Interface[55,56]

C_{load} leads to a higher path loss. On the other hand, resistive termination exhibits high-pass characteristics due to the resistance and return capacitance. It can be modeled as a high-pass filter with a cutoff frequency given by $f_c = \frac{1}{R_{load}C_{ret}}$[55].

At higher frequencies beyond the EQS band,

HBC Electrode: Ag/AgCl wet electrode is the most commonly used electrode in bio-electric signal monitoring[57,58]. This electrode offers advantages such as good contact with the skin, low contact impedance, affordability, high stability, and ease of fabrication[57,58]. Another type of electrode widely employed is the metal plate dry electrode, which exhibits good conductivity and is often utilized for capacitive coupling of signal energy into the body.

Fig. 3(c) shows a circuit representation for the skin-electrode interface[59]. The skin-electrode contact impedance is subject to variation due to factors such as human motion and postures, the presence of an air gap between the electrode and the skin, dehydration of wet electrodes, sweat and hair between the skin and electrodes, as well as dynamic environmental conditions. Thus, it is important to continuously monitor and compensate for the skin-electrode contact impedance to mitigate its influence on the channel. Fig. 3(c) shows the equivalent circuit model of the HBC electrode[53,55]. As the distance between the skin and the electrode increases, the capacitance decreases, resulting in a variable time constant that is determined by the product of its value and the electrode resistance.

Operational Frequency: The operational frequency is a crucial factor influencing various aspects of HBC, including channel characteristics, data rate, interference avoidance, and system stability. While the frequency range of interest for HBC is typically 10 kHz to 100 MHz, there is no consensus on the operational frequency used in transceiver architectures, and designs often do not adhere to the 5.25 MHz bandwidth centered at 21 MHz recommended by the IEEE 802.15.6 standard[32]. This will be discussed in detail in Section 4.

At EQS bands, the wavelength is orders of magnitude larger than the human body size, and the signal propagates within the body due to the skin's higher impedance compared to underlying layers. The near field operation, i.e., voltage transfer mode, is suitable for low-frequency transmission (biomedical data, etc.) and short-distance communication[60]. As the frequency increases to tens of MHz or higher, the far-field model becomes more appropriate to describe signal transmission. On-body communication can be characterized by the propagation of dipole source electric fields[60]. Compared to near-field EQS propagation, far-field surface waves propagate along the skin's surface. Far-field communication offers higher bandwidth, enabling larger data rates and longer distance transmissions[61]. However, at higher frequencies, impedance matching becomes necessary due to the comparable wavelength and circuit dimensions. Impedance matching optimizes the path loss and the received SNR at a specific frequency by reducing the reflected power, therefore power-mode transmission is usually considered instead of voltage-mode transmission. As frequency increases, severe signal leakage results in the propagation channel shifting from the human body to the surrounding air, and inter-device coupling plays a larger role in determining the path loss[62].

Interference to HBC systems occurs due to the presence of other communication systems close to or within HBC bands, such as cordless phones (46-50 MHz), frequency-modulated (FM) radio (88-108 MHz), walkie-talkies in the family radio service band (462-467 MHz), and NFC and RFID operating at 13.56 MHz[63]. These systems can cause interference that degrades communication reliability when their signals are injected into the human body through the body antenna effect. Therefore, it is crucial to account for such interference in the design of HBC transceivers.

Impulse Response Method The impulse response method is another approach used for characterizing the human body channel. This method involves applying customized channel-sounding signals to the human body using a battery-powered device and measuring the power of the received signal under various conditions. Measurement results include metrics such as mean path loss (MPL), BER, and frame error rate (FER), among others[64]. Other work analyzes other channel parameters, including root mean square (RMS) delay spread, mean and maximum excess delays (EDs), and MPL, for 52 different measurement conditions that involved varying device locations and body gestures[65]. The body channel transfer functions were derived using an adaptive filter approach based on iterative minimization of mean squared error. Additionally,[66] explored the body channel model between a wearable device on the wrist and an implantable device on the head based on measured body impulse responses. By considering different device locations and body postures, the variations of average RMS delay spread and maximum path gains were found to be 7 ns and 8 dB, respectively. These studies highlight the effectiveness of the impulse response method in analyzing the human body channel and provide valuable insights into the channel characteristics under various measurement conditions.

3.2 HBC Safety Standards

To guarantee the safety of humans exposed to electromagnetic fields, relevant standards are enacted by international institutions such as International Commission on Radiation Protection (ICNIRP)[12,13,32,67] and the IEEE C95.1 safety standard[12]. These standards specify constraints for contact current, field intensity limits for exposure to electromagnetic fields, and SAR with exposure to a magnetic field up to 300 GHz. For example, the IEEE 802.15.6 standard[32] specifies the parameters of short-range and wireless communication inside or around the human body. These standards also include limits for the skilled staff working

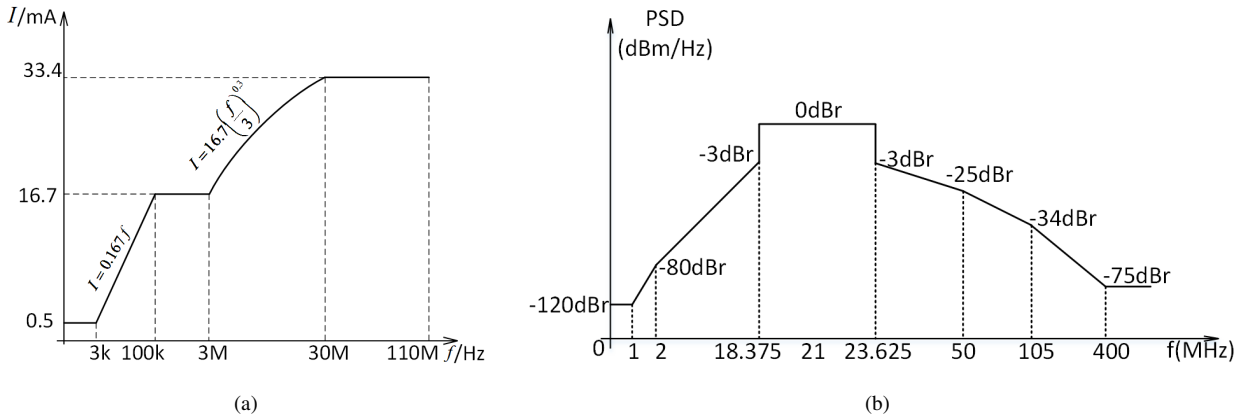

Figure 4. (a)Contact RMS current restriction by IEEE C95.1[12] and (b) The spectral mask specified by IEEE 802.15.6 standard[32].

in a restricted environment and the general public. The supplementary materials contain more information about the standards and safety limits.

For eHBC systems, electric field and contact current are considered to ensure that the conducted current along the human body is below the safety limit. An excessive contact current can cause pain and damage nerves or tissues. The IEEE C95.1 standard defines touch and grasping contacts between the human body and an energized conductor as firm electrical connections with a contact area of 1 cm^2 and 15 cm^2, respectively. Neither of these definitions perfectly describes a user who uses an HBC device. Nevertheless, the most conservative value of these limits can be considered as a ceiling value for any HBC device, as shown in Fig. 4(a). The contact current specified in this standard applies to a freestanding individual insulated from the ground and touching a grounded conductive object. In this case, the induced current limit applies to the situation where an individual only has conductive contact with the ground through the feet. A typical metric is the RMS current averaged over 0.2 s. For the contact voltage, the empirically determined value is 140 V which the U.S. Navy has used as a limit for RF signals to avoid arcing conditions, which is hardly achievable in HBC and out of concern. In addition to contact current limitations, the adverse effect resulting from the current is also influenced by the contact skin area. A larger contact area can reduce the adversarial effects, whereas a smaller contact area causes a higher tissue current density, making the skin heating more severe. It is reported that a painful heat sensation can be caused when the contact current is 46 mA within the frequency range of 100 kHz and 10 MHz and the exposure duration over 10s. The ICNIRP guideline specifies a 10 mA and 20 mA contact current limit for children and adults, respectively[13]. It is important to note that most reported eHBC implementations are well below the safety standards, with injected current per electrode in the μA's.

Controlling the intensity of electric field exposure in eHBC on body tissues is crucial due to potential adverse effects such as electrostimulation and heating. Electrostimulation occurs up to 5 MHz, while heating effects become significant above 100 kHz. Therefore, concerns up to 100 kHz primarily involve electrostimulation, with both electrostimulation and heating being pertinent in the frequency range of 100 kHz to 5 MHz[12]. To mitigate these risks, standards establish limits on the in-situ electric field strength across various body parts for frequencies between 0 and 5 MHz. These standards apply uniformly to whole-body exposure to sinusoidal, non-sinusoidal, and pulse electric fields, with an averaging period set at 30 minutes[12]. It's important to note that adhering to whole-body exposure limits may not guarantee compliance with local exposure limits; the stricter of the two should be adhered to in cases of discrepancy. Furthermore, in scenarios where multiple HBC devices operate simultaneously, generating multiple uncorrelated electric fields, compliance is assessed by summing the applicable field strength and power density percentages, which collectively should not exceed 100%.

Additionally, the IEEE 802.15.6 standard specifies the power spectrum density (PSD) for the standard mask in a frequency band centered at 21 MHz with a bandwidth of 5.25 MHz[32]. This standard also stipulates that the electric field strength at a distance of 30 m in free space should not exceed 30 μV/m, and the transmit power must be limited to ensure safety and minimize interference. Federal Communication Commission (FCC) limits more specifically regulate the electric field intensity around both unintentional and intentional radiators.

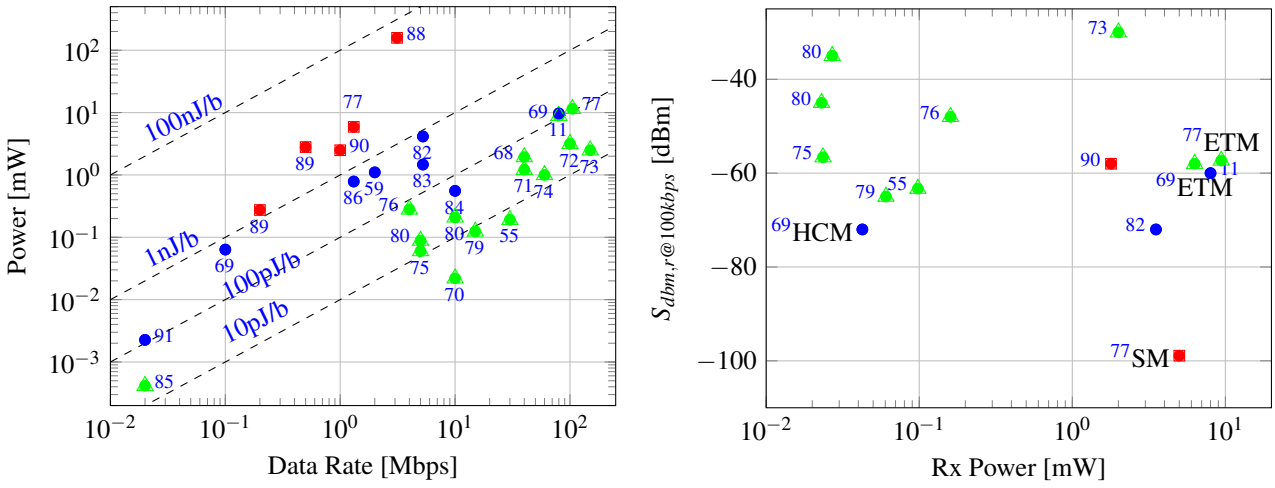

(a) (b)

Figure 5. (a) Summary of architecture performances showing the three classes of energy efficiency. Red square boxes indicate energy efficiency $>$ 1nJ/b; blue solid circles indicate energy efficiency lies between 100 pJ/b and 1 nJ/b; green triangles indicates energy efficiency 100 $<$ pJ/b (b) the receiver power versus the normalized sensitivity to 100 kbps reference data rate.

4 Key Transceiver Design Strategies

Several HBC transceiver architectures have been proposed to target various HBC specific design goals. Table 2 offers a representative quantitative summary of CC-HBC transceivers, including details such as modulation, frequency, data rate, power consumption, sensitivity, chip area, and BER. The architectures presented cover a diverse range of parameters, with transmission frequencies ranging from 1 MHz to 550 MHz, data rates spanning from 10 Kbps to 150 Mbps, and receiver sensitivities varying from -18.87 dBm to -98.9 dBm. Each architecture targets a specific design consideration within the extensive HBC design space. In this section, we present an in-depth discussion of the design strategies used to achieve efficient HBC transceivers.

4.1 Low Power Designs

Lifetime maximization of IoB nodes is crucial for battery-powered HBC transceivers. Based on energy efficiency, HBC architectures can broadly be categorized into three clusters: high, medium, and low energy-efficient architectures, which we set to correspond to energy consumption of less than 100 pJ/bit, greater than 100 pJ/bit, and less than 1 nJ/bit, and greater than 1 nJ/bit, respectively. Fig. 5(a) provides a visual summary of the data presented in Table 2. Depending on design choices made, some architectures achieve high energy efficiency while others are comparable to RF-based solutions.

We take sensitivity as an important metric to compare transceiver designs, as it sets the minimum input signal power required to produce a specified SNR ratio at the output port of the receiver. Sensitivity is thus a proxy for the quality of the receiver. Furthermore, sensitive receivers require lower transmission power thus reducing the overall network transmitted power, which is advantageous from a safety and security point of view. However, the cost of high sensitivity is typically higher circuitry power consumption. Fig. 5(b) shows the receiver power versus the normalized sensitivity for 100 kbps reference data rate. Normalized sensitivity is defined as $S_{dBm,r} = S_{dBm} - 10\log_{10}(D/r)$, where D is data rate, r is the reference data rate. The choice of 100 kbps as the reference data rate is arbitrary, selected as a basic data rate considered sufficient for the transmission of vital signals. The figure shows that there is a trade-off between sensitivity and Rx power, where a lower sensitivity results in higher Rx power consumption.

Duty Cycling and Resource Sharing Power-saving techniques such as duty cycling and resource sharing are commonly employed in HBC transceiver architectures to optimize power consumption and maximize component utilization. Duty cycling (a.k.a. power gating) involves periodically turning on and off specific components or functions to reduce overall power consumption. On the other hand, resource sharing allows multiple components or functions to share common resources, thereby optimizing their utilization and minimizing power consumption. Typical components that could be shared include oscillators, phase-locked loop (PLL), etc.[69,77,78]. In some designs, duty cycling is implemented through wake-up mechanisms. For instance, the power-expensive envelope detector and the injection locking oscillator may be shared in the main receiver in both Amplitude Shift Keying (ASK) and frequency shift keying (FSK) paths[92]. The wake-up RX operates in stand-alone mode when no data is received and is enabled only after receiving data. Finally, the operation is handed over to the main receiver.

Table 2. Summary of transceiver architectures

Energy Efficiency	Paper	Year	Modulation	Frequency [MHz]	Data Rate [Mbps]	Power [mW]		Energy Efficiency [J/bit]		Sensitivity [dBm]	Area [mm^2]	Process [nm]	Bit Error Rate	Coupling
						Tx	Rx	TX	RX					
HIGH	[68]	2015	WBS	1-80	1-40	1.94		48.5p		-36	0.04	90	$< 10^{-8}$	CC
	[69] ETM	2016	BPSK	20-60, 140-180	5-80	1.7-2.6	6.3	78.8p		-58	5.76	65	10^{-5}@ 40Mbps	CC
	[70]	2016	Manchester code	N/A	10	0.022		2.2p		N/A	N/A	N/A	N/A	CC
	[71]	2018	Walsh code	N/A	1-40	1.21		30.25p		-29	0.14	90	10^{-8}@40Mbps	CC
	[55]	2018, 2019	NRZ	bodywire	30	0.093	0.098	3.1p	3.27p	-63.3	0.122	65	N/A	CC
	[72]	2019	BRZ	1-100	100	0.475	2.68	4.75p	26.8p	N/A	1.2577	180	10^{-9}@0.5mA TX current	GC
	[73]	2018, 2020	OOK	150	150	0.49	2	16.6p		-30dBm@10^{-6}	0.00558	65	N/A	CC
					100	0.35		23.5p					N/A	CC
	[74]	2019	Hamming FSK	4-80	60	1		16.7		N/A	N/A	65	N/A	CC
	[75]	2019	OOK	37.5-42.5	5	0.0367	0.0235	7.15p	4.7p	-56.6	1	65	N/A	MC
	[76]	2019	OOK	21	4	0.12	0.16	70p		-48	2.8	180	$< 10^{-5}$	CC
	[77] ETM	2019	QPSK	31.5-52.5; 147-189	21/ 84	2.1	9.4	90p		-57.3	14.44	180	N/A	CC
	[78]	2020	OOK	1 (SC) 10 (HP)	22.27	0.0206 (SC) 0.0224 (HP)	N/A	20.6 (SC) 2.24 (HP)	N/A	N/A	0.117	65	N/A	CC
	[79]	2022	OOK and CPPM	20	7.5-15	0.0633	0.0606	4.2	4	-65(OOK), -52 (CPPM) @ 10^{-3} BER	0.3456	65	N/A	CC
	[80]	2022	GMSK	40-100	5	0.0655	0.023	15.5	4.6	-45	N/A	65	N/A	MC
			PAM4		10	0.182	0.027	19.4	2.7	-35	N/A			
MEDIUM	[69] HCM	2015, 2016	OOK	13.56	0.01-0.1	0.021	0.0425	430p		-72dBm	0.1672	65	10^{-5}@100kbps	CC
	[81]	2016	FSK	32-40	0.2	0.13	N/A	650p	N/A	N/A	0.273	130	N/A	CC
	[59]	2016, 2017	P-OFDM BPSK	20-120	0.2-2	1.1		550p		-83.1	0.542	65	10^{-7} @ 2Mb/s 10^{-10} @ 200kb/s	CC
	[82]	2017, 2019	BPSK	21	0.656-5.25	0.62	3.52	118p	670p	-72	0.6724	65	$< 10^{-7}$	CC
	[11]	2019	QPSK BPSK	20-60; 100-180	80	0.8-1.7	8	22p	100p	-60@80Mbps	NA	NA	10^{-5}@ 40Mbps	CC
	[83]	2019	Autoencoder	42	5.25	1.468		280p		N/A	0.116	45	N/A	CC
	[84]	2021	3-level clock embedded direct digital	40.68	10 (uplink) 0.2(downlink)	0.46	0.095	46p	470p	N/A	1.27	180	N/A	CC
	[85]	2021	OOK	0.05-1	Up to 0.02	0.000237	0.000178	11.85	8.9	-64@BER$< 10^{-3}$	0.17	65	N/A	CC
	[86]	2022	FSDT	N/A	1.312	0.647	0.137	493	105	N/A	0.17513	90	N/A	CC
	[87]	2022	NRZ	N/A	30-50	N/A	N/A	33.72	68.84	N/A	0.036	28	$< 10^{-3}$	CC
LOW	[88]	2020	WBS	N/A	0.78-3.125	77	81	24.64n	25.92n	-18.87	N/A	N/A	$< 10^{-8}$	CC
	[89] HI	2017	FSK RX	20/40	0.5	2.8		5.6n		-75	5.9925	180	N/A	CC
	[89] NI	2017	OOK RX, FSK TX	20	0.2	0.274		1.37n		-70	4.7	180	N/A	CC
	[77] SM	2019	BPSK	18.375-13.625	0.164-1.313	0.9	5	3.8n		-98.9	14.44	180	N/A	CC
	[90]	2020	DPFSK	80	1	0.7	1.79	0.7n	1.79n	-58@BER$< 10^{-3}$	0.46	180	N/A	CC
	[91]	2022	OOK	0.5-2	Up to 0.02	0.0013 (10p) 0.0015 (20p) 0.00219 (30p)	0.000072	109.5n	3.6p	-60@BER10^{-5}	0.0378	65	N/A	CC

ETM is entertainment (ET) mode. HCM is healthcare (HC) mode, HI is hub IC. NI is node IC. LP is low power. MU is multi-user. SM is standard mode. HP is high performance. WBS is wideband signaling. NRZ is non-return-to-zero. BRZ is bipolar return-to-zero. N/A is not available.

Low Power Building Blocks Various techniques can be employed to achieve low hardware complexity which directly leads to lower power transceivers. For instance, single-ended structures and simplified processes are utilized to realize low hardware complexity[82]. Another approach is to replace bulky and power-consuming crystal oscillators by employing crystal-less designs. For example, injection-locked (IL) oscillators as frequency dividers, are used to replace power-consuming PLLs[89]. This approach, coupled with the reuse of the received signal strength indicator (RSSI) for on-off keying (OOK) demodulation, results in significant reduction in power.

Other approaches to reduce power include; a) utilizing frequency domain processing[59] via efficient FFT/IFFT structures, b) using pulse-shaping with an injection locking ring oscillator and analog-to-digital (ADC) converter for sinewave modulation[11], delivering lower power consumption compared to PLL and Wien bridge implementations, c) using adiabatic communication for low power consumption[79], and d) using combinatorial pulse position modulation (CPPM) to improve energy efficiency, among others.

Architectural choices that contribute to reduced complexity include direct conversion architecture[77], direct envelope-detector-based RX architecture[75], and discrete-phase FSK (DPFSK) architecture utilizing a single PLL instead of continuous-phase FSK (CPFSK) with multiple PLLs and oscillators[90]. These approaches improve hardware complexity while maintaining functionality.

Energy Harvesting Energy scavenging harnesses ambient energy through various state-of-the-art technologies including thermoelectric generators for body heat conversion, piezoelectric devices for mechanical motion, triboelectric nanogenerators, biochemical processes, and RF energy harvesting. Advances in this field feature flexible materials and hybrid systems that combine multiple harvesting methods to improve efficiency and reliability[93]. Recent innovations in body-coupled ambient electromagnetic energy harvesting have shown potential in powering HBC systems without the need for high input voltage or complex setups, offering lower path loss compared to traditional RF transmission[57]. Additionally, there have been developments in HBC systems that facilitate simultaneous power and data transfer using advanced technologies such as Resonant EQS-HBC with maximum resonance power tracking and device capacitance cancellation[91]. Other notable advancements include tri-mode buck-converters for photovoltaic energy[94], single-inductor dual-output boost converters for thermoelectric harvesting[95], single-inductor piezoelectric harvesters[96], and dual input buck converters for triboelectric energy harvesting[97]. These techniques represent significant progress in efficiently powering HBC systems.

4.2 Return Path Compensation and Equalization

To enhance channel quality and design reliable HBC transceivers, return path compensation and equalization techniques are essential. An auto-loss compensation system was proposed that uses 5-bit digitally-controlled inductors to adjust the resonant frequency of an LC tank to match the carrier frequency[56,98]. Tuning is regulated by a proportional-integral controller. Using a capacitive termination at the LNA of the receiver expands the bandwidth and prevents the compensation strength from deterioration due to the resistive interface[76]. Self-adaptive compensation can be achieved by estimating the capacitance between transceivers based on their ground electrode distance using a backward capacitance model coupled with digitally-controlled tunable inductors to adjust for varying capacitances[99].

In terms of equalization, a decision feedback equalization scheme with eight taps was employed to address low-frequency path loss, thereby improving bandwidth and reducing inter-symbol interference[73]. Additionally, other work uses a shunt capacitor tuning in a complex filter to counteract center frequency drift caused by environmental changes, enhancing channel selection accuracy[100].

4.3 Environmental Variation and Human Motion Compensation

To address the challenges posed by varying human motion, postures, and environmental changes, compensation techniques typically focus on detecting, compensating, and calibrating based on path variations caused by variable contact impedance in eHBC. To monitor the contact impedance and compensate for the resulting loss, an RC relaxed contact impedance monitor could be used[59]. This monitor utilizes different time constants obtained from various suspension distances to detect impedance changes that are used to adjust the LNA gain. Contact impedance sensors[11] were introduced to mitigate the influence of contact impedance on distance measurements between transceivers, where the sensor continuously switches between the HBC mode and impedance sensing mode. It operates on chopper modulation principles, with impedance measurements based on the level of the chopper-demodulated and filtered signal. The sensor reliably covers contact impedance up to $1k\Omega$. To ensure robustness against environmental changes, a wideband signaling receiver was proposed[101], with a self-tuning circuit for each threshold voltage tuning branch, enabling the hysteresis threshold voltage of the Schmitt trigger to remain stable under changing environmental conditions.

4.4 System Reliability

The HBC system reliability is crucial for its successful operation in various applications and conditions. To ensure consistent and dependable communication, several techniques are employed to enhance overall system reliability, which are explored throughout this section.

Clock Reliability: To ensure reliable operation, the frequency of oscillators in HBC transceivers needs to be monitored and calibrated in real time. IL oscillators commonly utilize oscillator delay cells to automatically calibrate the operation frequency to the free-running frequency[11]. Self-calibrated voltage-controlled oscillators are used to maintain the oscillation frequency within the normal range[81].

Voltage Offset Calibration: Voltage offset can occur in single-ended circuits or due to the skin-electrode contact interface. When using a single-ended structure on the receiver side, the receiver chain may experience saturation due to DC offset[82]. To mitigate this, a self-calibration technique is employed to reduce the deviation of the DC point at the receiver side. This involves selecting the output of the low pass filter (LPF) first stage as an inner node, detecting it, and providing feedback to the front-end amplifier for automatic adjustment of its DC point. Another approach involves down-converting the received signal and up-converting the polarization voltage induced by the electrode-skin interface and DC offset of the front-end circuit[90]. The up-converted polarization voltage and DC offset are then filtered by a subsequent limiting amplifier, which also increases the amplitude of the demodulated baseband signals.

Coding Schemes: Employing effective coding schemes can enhance system reliability by achieving low jitter, improved synchronization, low BER, and scalability. For example, Manchester coding incorporates clock information within the coded data and provides better noise immunity[70]. This coding scheme improves time synchronization between the transmitter and receiver, thereby enhancing data transmission reliability. The reconfigurable Hamming coding scheme can be employed[74], resulting in up to 7x increase in data rate compared to traditional HBC coding. This coding scheme allows the transceiver to operate within a wide channel range, from 40 MHz to 100 MHz. To prevent DC offset build-up, a bipolar return to zero (BRZ) coding scheme is adopted[72]. Furthermore, AES encryption coding is applied to enhance security performance in HBC systems[85].

4.5 Noise and Interference Suppression

Different frequency bands offer varying levels of interference resistance and noise immunity. For instance, the near-field EQS band is suitable for short-distance and low-frequency communication, exhibiting less sensitivity to human gestures and environmental variations, resulting in higher bandwidth and reduced interference[60,61]. Surface wave propagation within specific frequency ranges, such as 350MHz to 550MHz[61] or 402MHz to 614MHz[100], has also been utilized, offering decreased interference compared to other transmission methods. Adaptive frequency hopping techniques have been employed over multiple channels to improve interference resistance and compensate for varying backward paths[59,63,85]. By carefully selecting frequency bands and employing frequency hopping mechanisms, interference from sources such as FM radio can be avoided[11,69].

Noise Filtering Various filtering techniques have been employed to enhance signal quality in HBC systems. For example, matched filter-based reshaping processes have been utilized for noisy channel mitigation, accompanied by phase error detection and correction schemes[102]. Additionally, employing steep roll-off filters helps suppress interference at specific frequency bands, particularly in cases where it may disrupt low-frequency vital signals[82]. Moreover, adaptive duty cycle integration techniques act as notch filters used to separate the desired signal from interfering noise in the time domain[55]. Decision feedback equalization with multiple taps compensates for low-frequency path loss and eliminates inter-symbol interference[73]. In the signal processing domain, mixing techniques are utilized to up-convert polarization voltage and DC offset, which are then filtered out by limiting amplifiers during down-conversion of the received signal to the baseband[90].

Mask Realization The IEEE 802.15.6 standard specifies a mask shown in Fig. 4(b). Several standard-compatible transceiver architectures have been proposed to meet the standard mask requirements. An active digital-bandpass filter (ADF) was proposed, consisting of an 8th-order bandpass filter implemented with a Butterworth infinite impulse response (IIR) filter, an 8-to-256 decoder, and a thermometric digital-to-analog converter (DAC)[103]. A second-order intermodulation cancellation technology was proposed for the body surface driver in the low-frequency band[104]. This technique effectively meets the stringent requirement for the transmit spectral mask, achieving a mask of -122 dBr at 1 MHz. Another approach uses an analog active filter instead of a DAC[105] to achieve wider bandwidth at lower power. Another work proposes using an IIR and a bandpass filter with a fifth-order high pass and a third-order low pass to improve mask rejection at frequencies lower than 2 MHz for the binary phase shift keying (BPSK) stream[106]. In addition, using a sigma-delta modulator to replace the DAC reduces the precision to 8 bits instead of 14 bits.

5 Future Research Trends

This section aims to outline potential directions for future research in the field of HBC.

5.1 Implantable HBC

Implantable HBC systems facilitate interactions between internal devices and external equipment, presenting significant advancements in medical technology. These systems, however, encounter numerous challenges that must be addressed through research focused on channel properties characterization and electrode design, essential for optimizing communication and ensuring reliable data transmission despite power constraints[107]. Biocompatibility and device longevity are critical, given the invasive nature of surgical replacements and the potential for adverse reactions. Additionally, developing secure communication protocols that operate under power and bandwidth limitations is crucial, especially considering the sensitive nature of the transmitted medical data. Addressing ethical issues such as patient consent and data ownership also remains a vital concern in the deployment of implantable HBC systems.

5.2 Deep Learning Solutions

Deep learning (DL) is transforming HBC through enhanced channel modeling, signal processing, data transmission optimization, and security improvements. Convolutional neural networks (CNNs) play a crucial role by filtering noise and improving signal clarity, which is vital for reliable data transmission across human body channels. DL algorithms also adapt to fluctuating channel conditions to optimize data rates, thus enhancing energy efficiency and throughput. A notable innovation is the integration of end-to-end autoencoders in HBC[108]. These autoencoders compress high-dimensional data into compact formats, easing data transmission over HBC's limited bandwidth. This compression is especially beneficial for transmitting complex physiological data effectively. Autoencoders also excel in noise reduction and feature extraction from raw HBC signals, facilitating accurate activity recognition and health state diagnostics by focusing on essential data characteristics and eliminating noise. This capability is critical for precise monitoring and diagnostic applications, further boosting the signal quality and reliability of HBC systems[108].

5.3 Ultra-thin Soft Electronics

Future research on HBC systems can be built on ultra-thin, flexible, and breathable electronic skin substrates, offering significant benefits in wearability and comfort. These substrates, being bio-compatible and merely several micrometers thick, ensure tight skin-device contact, which minimizes motion artifacts and enhances skin breathability. The close conformity to the skin's contours allows for more accurate and reliable collection of biometric data, such as heart rate and skin temperature, facilitating minimal intrusion and discomfort[109]. This advancement is key to enabling continuous, real-time health monitoring, which can aid in the early detection of health issues and provide personalized healthcare insights.

Beyond health monitoring, these technologies have potential applications in interactive wearable technology that can react to touch, temperature shifts, or the chemical makeup of sweat, offering innovative forms of user interaction and feedback. Such capabilities could particularly benefit athletes by providing real-time insights into physiological states and performance, or individuals with health conditions by offering immediate access to vital health information via wearable devices.

However, the broad implementation of ultra-thin soft electronics in HBC faces several challenges, including issues related to long-term durability, power consumption, and data processing capabilities. Additionally, integrating these devices with current medical and communication systems, while ensuring user privacy and data security, remains a significant obstacle.

5.4 Semantic Communication for HBC

The integration of semantic communication into Human Body Communication (HBC) represents a transformative approach by emphasizing the transmission of the "essence of the information" rather than raw data, enhancing the efficiency, intelligence, and contextual awareness of HBC systems. By focusing on semantically significant information, this approach reduces bandwidth and power consumption, addressing unreliability issues such as interference and signal attenuation in HBC channels[110]. Moreover, semantic communication's contextual awareness can revolutionize personalized healthcare and wearable technologies, enabling devices to prioritize critical health alerts and adjust operations based on the user's physical state or environment. However, implementing semantic communication in HBC requires advanced semantic encoding and decoding algorithms, necessitating further advancements in artificial intelligence and machine learning, as well as robust privacy and security measures to protect sensitive information.

References

1. Celik, A., Salama, K. N. & Eltawil, A. M. The internet of bodies: A systematic survey on propagation characterization and channel modeling. *IEEE Internet Things J.* **9**, 321–345, DOI: 10.1109/JIOT.2021.3098028 (2022).

2. Lutze, R. & Waldhör, K. Personal health assistance for elderly people via smartwatch based motion analysis. In *2017 Int. Conf. Healthc. Inform. (ICHI)*, 124–133, DOI: 10.1109/ICHI.2017.79 (2017).

3. Jones, R. W. A smart body area network for diabetes management. In *2019 22th Int. Conf. Inf. Fusion (FUSION)*, 1–8 (2019).

4. Huang, J. C.-S., Lin, Y.-T., Yu, J. K.-L. *et al.* A wearable NFC wristband to locate dementia patients through a participatory sensing system. In *2015 Int. Conf. Healthc. Inform. (ICHI)*, 208–212, DOI: 10.1109/ICHI.2015.32 (2015).

5. Alim, O. A., Moselhy, M. & Mroueh, F. EMG signal processing and diagnostic of muscle diseases. In *2012 2nd Int. Conf. Adv. Comput. Tools Eng. Appl. (ACTEA)*, 1–6, DOI: 10.1109/ICTEA.2012.6462866 (2012).

6. Rajni, R. & Kaur, I. Electrocardiogram signal analysis - an overview. *Int. J. Comput. Appl.* **84**, 22–25, DOI: 10.5120/14590-2826 (2013).

7. Kiourti, A. & Shubair, R. M. Implantable and ingestible sensors for wireless physiological monitoring: A review. In *2017 IEEE Int. Symp. Antenna Propag. USNC/URSI Nat. Radio Sci. Meeting (AP-S/URSI)*, 1677–1678, DOI: 10.1109/APUSNCURSINRSM.2017.8072881 (2017).

8. Clark, G. *Cochlear Implants*, 422–462 (Springer New York, New York, NY, 2004).

9. Turksoy, K., Samadi, S., Feng, J. *et al.* Meal detection in patients with type 1 diabetes: A new module for the multivariable adaptive artificial pancreas control system. *IEEE J. Biomed. Heal. Inform.* **20**, 47–54, DOI: 10.1109/JBHI.2015.2446413 (2016).

10. Feder, B. & Zeller, T. Identity badge worn under skin approved for use in health care (2004).

11. Jang, J., Lee, J., Lee, K.-R. *et al.* A four-camera VGA-resolution capsule endoscope system with 80-Mb/s body channel communication transceiver and sub-centimeter range capsule localization. *IEEE J. Solid-State Circuits* **54**, 538–549, DOI: 10.1109/JSSC.2018.2873630 (2019).

12. IEEE standard for safety levels with respect to human exposure to electric, magnetic, and electromagnetic fields, 0 Hz to 300 GHz. *IEEE Std C95.1-2019 (Revision IEEE Std C95.1-2005/ Incorporates IEEE Std C95.1-2019/Cor 1-2019)* 1–312, DOI: 10.1109/IEEESTD.2019.8859679 (2019).

13. ICNIRP. ICNIRP guidelines for limiting exposure to electromagnetic fields (100 kHZ to 300 GHZ). *Heal. Phys.* **74**, 483–524 (2020).

14. Das, D., Maity, S., Chatterjee, B. *et al.* Enabling covert body area network using electro-quasistatic human body communication. *Sci. Rep.* **9**, 1–14 (2019).

15. Mao, J., Yang, H. & Zhao, B. An investigation on ground electrodes of capacitive coupling human body communication. *IEEE Trans. Biomed. Circuits Syst.* **11**, 910–919, DOI: 10.1109/TBCAS.2017.2683532 (2017).

16. Hall, P. S., Hao, Y., Nechayev, Y. I. *et al.* Antennas and propagation for on-body communication systems. *IEEE Antennas Propag. Mag.* **49**, 41–58, DOI: 10.1109/MAP.2007.4293935 (2007).

17. Chatterjee, B., Srivastava, A., Seo, D.-H., Yang, D. & Sen, S. A context-aware reconfigurable transmitter with 2.24 pj/bit, 802.15. 6 nb-hbc and 4.93 pj/bit, 400.9 mhz medradio modes with 33.6% transmit efficiency. In *2020 IEEE Radio Frequency Integrated Circuits Symposium (RFIC)*, 75–78 (IEEE, 2020).

18. Chatterjee, B., Mohseni, P. & Sen, S. Bioelectronic sensor nodes for the internet of bodies. *Annu. Rev. Biomed. Eng.* **25**, 101–129, DOI: 10.1146/annurev-bioeng-110220-112448 (2023). Https://www.annualreviews.org/doi/pdf/10.1146/annurev-bioeng-110220-112448.

19. Yang, D., Mehrotra, P., Weigand, S. & Sen, S. In-the-wild interference characterization and modelling for electro-quasistatic-hbc with miniaturized wearables. *IEEE Transactions on Biomed. Eng.* **68**, 2858–2869, DOI: 10.1109/tbme.2021.3082078 (2021). Https://doi.org/10.1109/tbme.2021.3082078.

20. Bouazizi, A., Zaibi, G., Samet, M. *et al.* Wireless body area network for e-health applications: Overview. In *2017 Int. Conf. Smart Monit. Control. Cities (SM2C)*, 64–68, DOI: 10.1109/SM2C.2017.8071260 (2017).

21. Hasan, K., Biswas, K., Ahmed, K. *et al.* A comprehensive review of wireless body area network. *J. Netw. Comput. Appl.* **143**, 178–198, DOI: 10.1016/j.jnca.2019.06.016 (2019).

22. Kang, T., Oh, K.-I., Park, H. *et al.* Review of capacitive coupling human body communications based on digital transmission. *ICT Express* **2**, 180–187, DOI: 10.1016/j.icte.2016.11.002 (2016). Special Issue on Emerging Technologies for Medical Diagnostics.

23. Khorshid, A. E., Alquaydheb, I. N., Eltawil, A. M. *et al.* Sensitivity of galvanic intra-body communication channel to system parameters. In Mucchi, L., Hämäläinen, M., Jayousi, S. & Morosi, S. (eds.) *Body Area Networks: Smart IoT and Big Data for Intelligent Health Management*, 150–160 (Springer International Publishing, Cham, 2019).

24. Alquaydheb, I. N., Khorshid, A. E. & Eltawil, A. M. Analysis and estimation of intra-body communications path loss for galvanic coupling. In Fortino, G. & Wang, Z. (eds.) *Advances Body Area Netw. I*, 267–277 (Springer International Publishing, Cham, 2019).

25. Khorshid, A. E., Eltawil, A. M. & Kurdahi, F. Intra-body communication model based on variable biological parameters. In *2015 49th Asilomar Conf. Signals Syst. Comput.*, 948–951, DOI: 10.1109/ACSSC.2015.7421278 (2015).

26. Ullah, S., Khan, P., Ullah, N. *et al.* A review of wireless body area networks for medical applications. *Int. J. Commun. Netw. Syst. Sci.* **02**, DOI: 10.4236/ijcns.2009.28093 (2010).

27. Callejón, M. A., Naranjo-Hernandez, D., Reina-Tosina, J. *et al.* Distributed circuit modeling of galvanic and capacitive coupling for intrabody communication. *IEEE. Trans. Biomed. Eng.* **59**, 3263–3269, DOI: 10.1109/TBME.2012.2205382 (2012).

28. Callejón, M. A., Naranjo-Hernández, D., Reina-Tosina, J. *et al.* A comprehensive study into intrabody communication measurements. *IEEE Trans. Instrum. Meas.* **62**, 2446–2455, DOI: 10.1109/TIM.2013.2258766 (2013).

29. Movassaghi, S., Abolhasan, M., Lipman, J. *et al.* Wireless body area networks: A survey. *IEEE Commun. Surv. Tutor.* **16**, 1658–1686, DOI: 10.1109/SURV.2013.121313.00064 (2014).

30. Khorshid, A. E., Alquaydheb, I. N. & Eltawil, A. M. Electrode impedance modeling for channel characterization for intra-body communication. In Fortino, G. & Wang, Z. (eds.) *Advances Body Area Netw. I*, 253–266 (Springer International Publishing, Cham, 2019).

31. Ghoneim, M. S., Mohammaden, A., Said, L. A. *et al.* A comparative study of different human skin impedance models. In *2021 38th Nat. Radio Sci. Conf. (NRSC)*, vol. 1, 271–277, DOI: 10.1109/NRSC52299.2021.9509823 (2021).

32. IEEE standard for local and metropolitan area networks - part 15.6: Wireless body area networks. *IEEE Std 802.15.6-2012* 1–271, DOI: 10.1109/IEEESTD.2012.6161600 (2012).

33. Bondok, A. H., El-Mohandes, A. M., Shalaby, A. *et al.* A low complexity UWB PHY baseband transceiver for IEEE 802.15.6 WBAN. In *2017 30th IEEE Int. SoC Conf. (SOCC)*, 262–267, DOI: 10.1109/SOCC.2017.8226054 (2017).

34. Witters, D. & Campbell, C. A. Wireless medical telemetry: Addressing the interference issue and the new wireless medical telemetry service (wmts). In Dyro, J. F. (ed.) *Clinical Engineering Handbook*, Biomedical Engineering, 492–497, DOI: https://doi.org/10.1016/B978-012226570-9/50113-7 (Academic Press, Burlington, 2004).

35. Pramanik, P. K. D., Nayyar, A. & Pareek, G. Chapter 7 - WBAN: Driving e-healthcare beyond telemedicine to remote health monitoring: Architecture and protocols. In D. Jude, H. & Balas, V. E. (eds.) *Telemedicine Technologies*, 89–119, DOI: https://doi.org/10.1016/B978-0-12-816948-3.00007-6 (Academic Press, 2019).

36. Bluetooth SIG Proprietary. *Bluetooth Core Specification* (2021).

37. Tosi, J., Taffoni, F., Santacatterina, M. *et al.* Performance evaluation of bluetooth low energy: A systematic review. *Sensors* **17**, DOI: 10.3390/s17122898 (2017).

38. Gupta, N. K. *Inside Bluetooth low energy* (Artech House, 2016).

39. Kumar, N. V. R., Bhuvana, C. *et al.* Comparison of zigbee and bluetooth wireless technologies-survey. In *2017 Int. Conf. Inf. Commun. Embed. Syst. (ICICES)*, 1–4, DOI: 10.1109/ICICES.2017.8070716 (2017).

40. Dementyev, A., Hodges, S., Taylor, S. *et al.* Power consumption analysis of bluetooth low energy, zigbee and ant sensor nodes in a cyclic sleep scenario. In *2013 IEEE International Wireless Symposium (IWS)*, 1–4 (IEEE, 2013).

41. Hito, M., Kuo, L., Newman, A. *et al.* Development of a portable z-wave signal detector for home security installations. In *2019 Systems and Information Engineering Design Symposium (SIEDS)*, 1–6, DOI: 10.1109/SIEDS.2019.8735588 (2019).

42. Dynastream Innovations. *CC2571* (2011).

43. Suresh, S. & Chakaravarthi, G. RFID technology and its diverse applications: A brief exposition with a proposed machine learning approach. *Measurement* **195**, 111197, DOI: https://doi.org/10.1016/j.measurement.2022.111197 (2022).

44. Mezzanotte, P., Palazzi, V., Alimenti, F. *et al.* Innovative RFID sensors for internet of things applications. *IEEE J. Microwaves* **1**, 55–65, DOI: 10.1109/JMW.2020.3035020 (2021).

45. Nordic Semiconductor. *nRF5340* (2021).

46. NXP semiconductor. *NTAG 424 DNA* (2019).

47. Silicon Labs. *EFR32ZG23* (2021).

48. Ieee standard for local and metropolitan area networks - part 15.6: Wireless body area networks. *IEEE Std 802.15.6-2012* 1–271, DOI: 10.1109/IEEESTD.2012.6161600 (2012).

49. Park, J. & Mercier, P. P. Magnetic human body communication. In *2015 37th Int. Conf. IEEE Eng. Med. Biol. Soc. (EMBC)*, 1841–1844, DOI: 10.1109/EMBC.2015.7318739 (2015).

50. Vasić, Ž. L., Cifrek, M., Gao, Y. & Du, M. Preliminary characterization of capacitive intrabody communication channel under implantable-like conditions. In *2020 IEEE International Instrumentation and Measurement Technology Conference (I2MTC)*, 1–5 (IEEE, 2020).

51. Ogasawara, T., Sasaki, A.-i., Fujii, K. *et al.* Human body communication based on magnetic coupling. *IEEE Trans. Antennas Propag.* **62**, 804–813, DOI: 10.1109/TAP.2013.2292705 (2014).

52. Park, J. & Mercier, P. P. Sub-40 μW 5 Mb/s magnetic human body communication transceiver demonstrating trans-body delivery of high-fidelity audio to a wearable in-ear headphone. In *2019 IEEE Int. Solid- State Circuits Conf. - (ISSCC)*, 286–287, DOI: 10.1109/ISSCC.2019.8662387 (2019).

53. Maity, S., He, M., Nath, M. *et al.* Bio-physical modeling, characterization, and optimization of electro-quasistatic human body communication. *IEEE. Trans. Biomed. Eng.* **66**, 1791–1802, DOI: 10.1109/TBME.2018.2879462 (2019).

54. Park, J., Garudadri, H. & Mercier, P. P. Channel modeling of miniaturized battery-powered capacitive human body communication systems. *IEEE. Trans. Biomed. Eng.* **64**, 452–462, DOI: 10.1109/TBME.2016.2560881 (2017).

55. Maity, S., Chatterjee, B., Chang, G. *et al.* Bodywire: A 6.3-pJ/b 30-Mb/s-30-dB sir-tolerant broadband interference-robust human body communication transceiver using time domain interference rejection. *IEEE J. Solid-State Circuits* **54**, 2892–2906, DOI: 10.1109/JSSC.2019.2932852 (2019).

56. Zhao, J., Sun, W., Mao, J. *et al.* An auto loss compensation system for capacitive-coupled body channel communication. *IEEE Trans. Biomed. Circuits Syst.* **13**, 756–765, DOI: 10.1109/TBCAS.2019.2923780 (2019).

57. Li, J., Dong, Y. *et al.* Body-coupled power transmission and energy harvesting. *Nat. Electron.* **4**, 530–538 (2021).

58. Khorshid, A. E., Alquaydheb, I. N. *et al.* Ibcfap: Intra-body communications five-layers arm phantom model. *Ieee Access* **7**, 93701–93710 (2019).

59. Saadeh, W., Altaf, M. A. B., Alsuradi, H. *et al.* A 1.1-mw ground effect-resilient body-coupled communication transceiver with pseudo ofdm for head and body area network. *IEEE J. Solid-State Circuits* **52**, 2690–2702, DOI: 10.1109/JSSC.2017.2713522 (2017).

60. Jang, J., Bae, J. & Yoo, H.-J. Understanding body channel communication : A review: from history to the future applications. In *2019 IEEE Cust. Integr. Circuits Conf. (CICC)*, 1–8, DOI: 10.1109/CICC.2019.8780224 (2019).

61. Tochou, G., Benarrouch, R., Gaidioz, D. *et al.* A Fully-Digital 0.1-to-27 Mb/s ULV 450 MHz Transmitter with sub-100 μW Power Consumption for Body-Coupled Communication in 28 nm FD-SOI CMOS. In *2021 IEEE Radio Frequency Integrated Circuits Symposium (RFIC)*, 195–198, DOI: 10.1109/rfic51843.2021.9490464 (IEEE, Atlanta, United States, 2021).

62. Avlani, S., Nath, M., Maity, S. & Sen, S. A 100khz-1ghz termination-dependent human body communication channel measurement using miniaturized wearable devices. In *2020 Design, Automation & Test in Europe Conference & Exhibition (DATE)*, 650–653, DOI: 10.23919/DATE48585.2020.9116556 (2020).

63. Cho, N., Yan, L., Bae, J. *et al.* A 60 kb/s–10 Mb/s adaptive frequency hopping transceiver for interference-resilient body channel communication. *IEEE J. Solid-State Circuits* **44**, 708–717, DOI: 10.1109/JSSC.2008.2012328 (2009).

64. Kang, T. *et al.* Measurement and analysis of electric signal transmission using human body as medium for wban applications. *IEEE Transactions on Instrumentation Meas.* **67**, 527–537 (2018).

65. Kang, T. *et al.* Evaluation of human body characteristics for electric signal transmission based on measured body impulse response. *IEEE transactions on instrumentation measurement* **69**, 6399–6411 (2020).

66. Kang, T. *et al.* Measurement and evaluation of electric signal transmission through human body by channel modeling, system design, and implementation. *IEEE Transactions on Instrumentation Meas.* **70**, 1–14 (2021).

67. ICNIRP. ICNIRP guidelines for limiting exposure to electromagnetic fields (1 Hz to 100 kHZ). *Heal. Phys.* **74**, 483–524 (2010).

68. Chung, C.-C., Chang, C.-T. & Lin, C.-Y. A 1 Mb/s–40 Mb/s human body channel communication transceiver. In *VLSI Des., Autom. and Test(VLSI-DAT)*, 1–4, DOI: 10.1109/VLSI-DAT.2015.7114536 (2015).

69. Cho, H., Kim, H., Kim, M. *et al.* A 79 pJ/b 80 Mb/s full-duplex transceiver and a 42.5 μW 100 kb/s super-regenerative transceiver for body channel communication. *IEEE J. Solid-State Circuits* **51**, 310–317, DOI: 10.1109/JSSC.2015.2498761 (2016).

70. Tseng, Y., Lin, T., Yau, S. *et al.* A 0.5 V/22 μ W low power transceiver IC for use in ESC intra-body communication system. In *2016 Int. SoC Des. Conf. (ISOCC)*, 71–72, DOI: 10.1109/ISOCC.2016.7799738 (2016).

71. Chung, C.-C., Chang, R.-H. & Li, M.-H. An FPGA-based transceiver for human body channel communication using Walsh codes. In *2018 IEEE Int. Conf. Consum. Electron.-Taiwan (ICCE-TW)*, 1–2, DOI: 10.1109/ICCE-China.2018.8448903 (2018).

72. Jeon, Y., Jung, C., Cheon, S.-I. *et al.* A 100 Mb/s galvanically-coupled body-channel-communication transceiver with 4.75 pJ/b TX and 26.8 pJ/b rx for bionic arms. In *2019 Symp. VLSI Circuit*, C292–C293, DOI: 10.23919/VLSIC.2019.8778040 (2019).

73. Lee, J.-H., Ko, J., Kim, K. *et al.* A body channel communication technique utilizing decision feedback equalization. *IEEE Access* **8**, 198468–198481, DOI: 10.1109/ACCESS.2020.3034999 (2020).

74. Vijayalakshmi, S. & Velmurugan, N. Design and implementation of low power high-efficient transceiver for body channel communications. *J. Med. Syst.* **43**, DOI: 10.1007/s10916-019-1204-x (2019).

75. Park, J. & Mercier, P. P. A Sub-10-pJ/bit 5-Mb/s magnetic human body communication transceiver. *IEEE J. Solid-State Circuits* **54**, 3031–3042, DOI: 10.1109/JSSC.2019.2935549 (2019).

76. Zhao, J., Mao, J., Sun, W. *et al.* A 4-Mbps 41-pJ/bit on-off keying transceiver for body-channel communication with enhanced auto loss compensation technique. In *2019 IEEE Asian Solid-State Circuits Conf. (A-SSCC)*, 173–176, DOI: 10.1109/A-SSCC47793.2019.9056946 (2019).

77. Jang, J., Cho, H. & Yoo, H.-J. An 802.15.6 HBC standard compatible transceiver and 90 pJ/b full-duplex transceiver for body channel communication. In *2019 IEEE Biomed. Circuits Syst. Conf. (BioCAS)*, 1–4, DOI: 10.1109/BIOCAS.2019.8919040 (2019).

78. Chatterjee, B., Srivastava, A., Seo, D.-H., Yang, D. & Sen, S. A context-aware reconfigurable transmitter with 2.24 pj/bit, 802.15. 6 nb-hbc and 4.93 pj/bit, 400.9 mhz medradio modes with 33.6% transmit efficiency. In *2020 IEEE Radio Frequency Integrated Circuits Symposium (RFIC)*, 75–78 (IEEE, 2020).

79. Chatterjee, B. *et al.* A 65nm 63.3μw 15 Mbps transceiver with switched-capacitor adiabatic signaling and combinatorial-pulse-position modulation for body-worn video-sensing ar nodes. In *2022 IEEE International Solid-State Circuits Conference (ISSCC)*, vol. 65, 276–278, DOI: 10.1109/ISSCC42614.2022.9731793 (2022).

80. Meng, M. *et al.* A gmsk/pam4 multichannel magnetic human body communication transceiver. *IEEE Solid-State Circuits Lett.* **5**, 66–69, DOI: 10.1109/LSSC.2022.3158691 (2022).

81. Wang, B., Shao, H. & Wang, C. A small-footprint body channal communication transceiver using only one phase-locked loop as modulator and demodulator. In *2016 14th IEEE Int. New Circuits Syst. Conf. (NEWCAS)*, 1–4, DOI: 10.1109/NEWCAS.2016.7604775 (2016).

82. Zhao, B., Lian, Y., Niknejad, A. M. *et al.* A low-power compact IEEE 802.15.6 compatible human body communication transceiver with digital sigma–delta IIR mask shaping. *IEEE J. Solid-State Circuits* **54**, 346–357, DOI: 10.1109/JSSC.2018.2873586 (2019).

83. Ali, A., Inoue, K., Shalaby, A. *et al.* Efficient autoencoder-based human body communication transceiver for WBAN. *IEEE Access* **7**, 117196–117205, DOI: 10.1109/ACCESS.2019.2936796 (2019).

84. Kim, B., Yuk, B. & Bae, J. A wirelessly-powered 10 Mbps 46-pJ/b body channel communication system with 45% PCE multi-stage and multi-source rectifier for neural interface applications. In *IEEE Asian Solid-State Circuits Conf. (A-SSCC)*, 1–3, DOI: 10.1109/A-SSCC53895.2021.9634761 (2021).

85. Maity, S. *et al.* Sub-μ wrcomm: 415-nw 1–10-kb/s physically and mathematically secure electro-quasi-static hbc node for authentication and medical applications. *IEEE J. Solid-State Circuits* **56**, 788–802, DOI: 10.1109/JSSC.2020.3041874 (2021).

86. Ali, A., Ahmed, S. M., Sayed, M. S. & Shalaby, A. Deep learning-based human body communication baseband transceiver for wban ieee 802.15.6. *Eng. Appl. Artif. Intell.* **115**, 105169, DOI: https://doi.org/10.1016/j.engappai.2022.105169 (2022).

87. Ko, J. *et al.* A 50 mb/s full hbc trx with adaptive dfe and variable-interval 3x oversampling cdr in 28nm cmos technology for a 75 cm body channel moving at 0.75 cycle/sec. In *ESSCIRC 2022- IEEE 48th European Solid State Circuits Conference (ESSCIRC)*, 213–216, DOI: 10.1109/ESSCIRC55480.2022.9911296 (2022).

88. Chung, C.-C., Sheng, D. & Li, M.-H. Design of a human body channel communication transceiver using convolutional codes. *Microelectron. J* **100**, 104783, DOI: https://doi.org/10.1016/j.mejo.2020.104783 (2020).

89. Lee, Y. & Yoo, H.-j. A 274 μW clock synchronized wireless body area network ic with super-regenerative RSSI for biomedical ad-hoc network system. In *2017 39th Int. Conf. IEEE Eng. Med. Biol. Soc. (EMBC)*, 710–713, DOI: 10.1109/EMBC.2017.8036923 (2017).

90. Shih, H.-Y., Chang, Y.-C., Yang, C.-W. *et al.* A low-power and small chip-area multi-rate human body communication DPFSK transceiver for wearable devices. *IEEE Trans. Circuits Syst. II Express Briefs* **67**, 1234–1238, DOI: 10.1109/TCSII.2019.2937746 (2020).

91. Modak, N. *et al.* Eqs res-hbc: A 65-nm electro-quasistatic resonant 5–240 μw human whole-body powering and 2.19 μw communication soc with automatic maximum resonant power tracking. *IEEE J. Solid-State Circuits* **57**, 831–844, DOI: 10.1109/JSSC.2022.3142177 (2022).

92. Jang, J., Lee, J., Cho, H. *et al.* Wireless body-area-network transceiver and low-power receiver with high application expandability. *IEEE J. Solid-State Circuits* **55**, 2781–2789, DOI: 10.1109/JSSC.2020.3005765 (2020).

93. Cavallari, R., Martelli, F., Rosini, R. *et al.* A survey on wireless body area networks: Technologies and design challenges. *IEEE Commun. Surv. Tutor.* **16**, 1635–1657, DOI: 10.1109/SURV.2014.012214.00007 (2014).

94. Chen, P.-H., Wu, C.-S. & Lin, K.-C. 20.10 a 50nw-to-10mw output power tri-mode digital buck converter with self-tracking zero current detection for photovoltaic energy harvesting. In *2015 IEEE International Solid-State Circuits Conference - (ISSCC) Digest of Technical Papers*, 1–3, DOI: 10.1109/ISSCC.2015.7063083 (2015).

95. Katic, J., Rodriguez, S. & Rusu, A. A dual-output thermoelectric energy harvesting interface with 86.6% peak efficiency at 30μ w and total control power of 160 nw. *IEEE J. Solid-State Circuits* **51**, 1928–1937 (2016).

96. Kwon, D. & Rincón-Mora, G. A. A single-inductor 0.35 μm cmos energy-investing piezoelectric harvester. *IEEE J. Solid-State Circuits* **49**, 2277–2291, DOI: 10.1109/JSSC.2014.2342721 (2014).

97. Park, I., Maeng, J., Shim, M., Jeong, J. & Kim, C. A high-voltage dual-input buck converter achieving 52.9% maximum end-to-end efficiency for triboelectric energy-harvesting applications. *IEEE J. Solid-State Circuits* **55**, 1324–1336, DOI: 10.1109/JSSC.2019.2942370 (2020).

98. Zhao, J. *et al.* An auto loss compensation system for non-contact capacitive coupled body channel communication. In *2018 IEEE International Symposium on Circuits and Systems (ISCAS)*, 1–5 (IEEE, 2018).

99. Mao, J., Yang, H., Lian, Y. *et al.* A self-adaptive capacitive compensation technique for body channel communication. *IEEE Trans. Biomed. Circuits Syst.* **11**, 1001–1012, DOI: 10.1109/TBCAS.2017.2695058 (2017).

100. Wang, Y., Zhang, C., Yuan, F. *et al.* A 402-614 MHz CMOS transceiver for ieee 802.15.6 wireless body area networks. In *2019 IEEE 4th IEEE 3rd Int. Conf. Integr. Circuits Microsyst. (ICICM)*, 210–214, DOI: 10.1109/ICICM48536.2019.8977187 (2019).

101. Lin, K., Wang, B., Xing, Z. *et al.* A novel low-power compact WBS human body channel receiver for wearable vital signal sensing application in wireless body-area network. *Microsyst. Technol.* **23**, DOI: 10.1007/s00542-016-3244-1 (2017).

102. El-Mohandes, A. M., Shalaby, A. & Sayed, M. S. Efficient low-power digital baseband transceiver for IEEE 802.15.6 narrowband physical layer. *IEEE Trans Very Large Scale Integr VLSI Syst.* **26**, 2372–2385, DOI: 10.1109/TVLSI.2018.2862348 (2018).

103. Lee, H. *et al.* A 5.5 mW IEEE-802.15.6 wireless body-area-network standard transceiver for multichannel electro-acupuncture application. In *2013 IEEE International Solid-State Circuits Conference Digest of Technical Papers*, 452–453 (IEEE, 2013).

104. Liu, Y., Zhao, B., Yang, Y. & Lian, Y. A novel hybrid two-stage IM2 cancelling technique for IEEE 802.15.6 HBC standard. In *2014 IEEE Biomedical Circuits and Systems Conference (BioCAS) Proceedings*, 640–643 (IEEE, 2014).

105. Cho, H., Lee, H., Bae, J. & Yoo, H.-J. A 5.2 mW IEEE 802.15. 6 HBC standard compatible transceiver with power efficient delay-locked-loop based BPSK demodulator. *IEEE journal solid-state circuits* **50**, 2549–2559 (2015).

106. Zhao, B., Lian, Y., Niknejad, A. M. & Heng, C. H. A low-power compact IEEE 802.15.6 compatible human body communication transceiver with digital sigma–delta iir mask shaping. *IEEE J. Solid-State Circuits* **54**, 346–357 (2018).

107. Muramatsu, D. & Kodama, M. Signal transmission analysis in implantable human body communication for abdominal medical devices. *AIP Adv.* **13** (2023).

108. Ali, A., Inoue, K., Shalaby, A., Sayed, M. S. & Ahmed, S. M. Efficient autoencoder-based human body communication transceiver for wban. *IEEE Access* **7**, 117196–117205 (2019).

109. Kim, D.-H., Lu, N., Ma, R. *et al.* Epidermal electronics. *science* **333**, 838–843 (2011).

110. Luo, X., Chen, H.-H. & Guo, Q. Semantic communications: Overview, open issues, and future research directions. *IEEE Wirel. Commun.* **29**, 210–219 (2022).